Studies of the universal contact in a strongly interacting Fermi gas using Bragg spectroscopy

Studies of the universal contact in a strongly interacting Fermi gas using Bragg spectroscopy

E D Kuhnle, S Hoinka, H Hu, P Dyke, P Hannaford and C J Vale[1]

ARC Centre of Excellence for Quantum-Atom Optics, Centre for Atom Optics
and Ultrafast Spectroscopy, Swinburne University of Technology,
Melbourne 3122, Australia
E-mail: cvale@swin.edu.au

Abstract.   We present a comprehensive experimental study of Tan's universal contact parameter $\mathcal{I}$ in a two-component ultracold Fermi gas, using Bragg spectroscopy. The contact uniquely parameterizes a number of universal properties of Fermi gases in the strongly interacting regime. It is linked to the spin-antiparallel component of the static structure factor $S_{\uparrow\downarrow}(k)$ at high momenta, which can readily be obtained via Bragg scattering. Contact depends upon the relative interaction strength $1/(k_{\mathrm{F}}a)$ and temperature T/T_{F}, where k_{F} is the Fermi wave vector, a is the s-wave scattering length and T_{F} is the Fermi temperature. We present measurements of both of these dependencies in a cloud of ^{6}Li atoms and compare our findings to theoretical predictions. We also compare Bragg spectroscopic methods based on measuring the energy and momentum transferred to the cloud and examine the conditions under which the energy transfer method provides improved accuracy. Our measurements of the dynamic structure factor and contact are found to be in good agreement with theoretical predictions based on the quantum virial expansion.

[1] Author to whom any correspondence should be addressed.

IOP Institute of Physics ⦿ DEUTSCHE PHYSIKALISCHE GESELLSCHAFT

Contents

1. Introduction

New insights into strongly interacting Fermi gases have emerged as an important development leading to new understandings of highly correlated systems of fermions. This universality means that any dilute Fermi system with sufficiently strong interactions will behave identically on a scale given by the average particle separation, independent of the details of the short range interaction. In a two-component Fermi gas, when the range of the scattering potential r_0 is much smaller than the mean interparticle spacing $n^{-1/3}$ and the s-wave scattering length a, which characterizes elastic collisions, is large, the system can display universal properties. Ultracold gases of fermionic atoms near a Feshbach resonance are an excellent system in which to access the universal regime in a precisely controlled manner [1–3]. With the discovery of universality in the Bose–Einstein condensate (BEC) to Bardeen–Cooper–Schrieffer (BCS) crossover, ultracold Fermi gases near Feshbach resonances have become a central topic in atomic physics [4–12]. Similar strongly interacting Fermi systems arise in a wide variety of physical settings, from astrophysical to nuclear and condensed matter systems. One can therefore study universality in ultracold atomic gases to help understand other strongly interacting Fermi superfluids, taking advantage of the ability to precisely control atom–atom interactions.

From a theoretical viewpoint, these strongly interacting Fermi gases can present significant challenges [13]. As the scattering length becomes large, it can no longer be treated as a small parameter and perturbative theories, which have had wide success for weakly interacting Bose gases, typically fail. In 2008, Shina Tan made dramatic progress by deriving several exact relations valid through the BEC-BCS crossover, which relate the microscopic properties to bulk thermodynamic quantities through a single parameter, $\mathcal{I}$, known as the contact [14–16]. These exact relations are applicable in broad circumstances: zero or finite temperatures, superfluid or normal phases, homogeneous or trapped systems and in few- or many-body systems. Contact is defined as

$$\mathcal{I} = \lim_{k \to \infty} n_k k^4, \tag{1}$$

where n_k is the momentum distribution of a single-spin component as a function of the wave vector k. At large k, n_k has a $1/k^4$ dependence, so the contact is a constant that depends on two-body interactions and quantifies the amplitude of this high momentum tail. A more physically

intuitive picture of the contact was also given by Tan as the number of closely spaced spin-up/spin-down pairs, i.e. $\mathcal{I}$ quantifies the likelihood of finding two fermions with opposite spin close enough to interact with each other. In systems with a large scattering length, where the range of the interaction potentials is negligible, this single parameter encapsulates all of the information required in order to determine the many-body properties [17, 18]. $\mathcal{I}$ depends on two quantities: the dimensionless interaction parameter $1/(k_{\mathrm{F}}a)$, where k_{F} is the Fermi wave vector, and the relative temperature of the system T/T_{F}, where T_{F} is the Fermi energy divided by Boltzmann's constant. We follow the notation introduced by Tan where $\mathcal{I}$ is the integrated contact density applicable to trapped gases ($\mathcal{I} = \int \mathcal{C}(\mathbf{r})\mathrm{d}^3 r$, where $\mathcal{C}(\mathbf{r})$ is the local contact density).

Tan showed that the internal energy of a gas across the BEC–BCS crossover can be expressed as a functional of the momentum distribution at k and that the pair correlation function diverges as $\mathcal{I}/r^2$ at short distance $r < 1/k_{\mathrm{F}}$ [14, 19]. Tan also derived the adiabatic relation $\mathrm{d}E/\mathrm{d}(-1/a) = \hbar^2 \mathcal{I}/(4\pi m)$, where m is the atomic mass, yielding the change in total energy E due to an adiabatic change in the scattering length [15], and extended the virial theorem to finite a and imbalanced spin populations [16].

Experimentally, the contact $\mathcal{I}$ was first extracted [20] from the number of closed-channel molecules determined through photo-association experiments [8]. More recently, $\mathcal{I}$ was measured both directly from the tail of the momentum distribution and using radio frequency (rf) spectroscopy by the JILA group [21]. The JILA group also experimentally verified Tan's adiabatic and virial relations [21]. Recent work by the ENS group obtained the contact at unitarity from the measured equation of state of a homogeneous gas [12]. Previous work in our group at Swinburne pointed out that Tan's universal relation for the pair-correlation function could be tested through measurements of the static structure factor $S(k)$ using Bragg spectroscopy [22].

Here, we show that Bragg spectroscopy can provide a good measure of the interaction and temperature dependences of the contact across a broad region of the Feshbach resonance. We also demonstrate a new experimental technique for determining the energy transferred by a Bragg pulse with good signal-to-noise ratio. Theoretical calculations based on the quantum virial expansion (QVE) are shown to agree with measurements of the dynamic structure factor and contact at temperatures down to $T \gtrsim 0.5T_{\mathrm{F}}$. This paper is organized as follows. In section 2, we give a detailed overview of how the contact can be measured using Bragg spectroscopy and the methods we use. In section 3, we present measurements of the interaction dependence of the contact extracted from our previous work on the static structure factor. In section 4, we report measurements of the temperature dependence of the contact. We first describe our techniques for setting and measuring the cloud temperature and then use a new method of energy transfer Bragg spectroscopy to measure the temperature dependence of the contact and compare these results to those obtained using traditional momentum transfer Bragg spectroscopy. The Bragg spectra are found to be in good agreement with QVE calculations for a range of temperatures and interaction strengths. In section 5, we summarize our findings and provide an outlook for future investigations.

2. Measuring contact using Bragg spectroscopy

Tan's exact universal relations, such as the adiabatic and virial theorems mentioned in the previous section, link many-body quantities such as the total energy and momentum distribution

to the the two-body scattering length through a single short-range parameter, the contact $\mathcal{I}$. The short-range structure in a quantum fluid depends upon the relative wave-function of the interacting particles, in this case fermions in different spin states. In a two-component (spin-up/spin-down) Fermi gas, this is given by $\psi_{\uparrow\downarrow}(r) \propto 1/r - 1/a$. Tan used this to show that, for length scales $r_0 < r < 1/k_{\mathrm{F}}$, the spin-antiparallel pair-correlation function is given exactly by equation (2), which includes the contact as a pre-factor [14],

$$g_{\uparrow\downarrow}^{(2)}(r) = \frac{\mathcal{I}}{16\pi^2} \left(\frac{1}{r^2} - \frac{2}{ar} \right). \tag{2}$$

Such pair-correlation functions are difficult to measure directly in ultracold gases; however, it is possible to measure macroscopic quantities that depend on the correlation functions in a well-defined way. A prime example is the static structure factor, $S(k)$, which is given by the Fourier transform of $g^{(2)}(r)$. In a two-component Fermi gas with an equal number of particles $N/2$ in each spin state, the structure factor contains two equally weighted contributions arising from correlations between particles in the same state and between particles in different states $S(k) = S_{\uparrow\uparrow}(k) + S_{\uparrow\downarrow}(k)$. When the probe momentum ($q = \hbar k$) is much larger than the Fermi momentum, particles in the same state will be uncorrelated and $S_{\uparrow\uparrow}(k \gg k_{\mathrm{F}}) \simeq 1$, so all variation in $S(k)$ will then be due to changes in $S_{\uparrow\downarrow}(k)$ [9, 19]. The Fourier transform of equation (2) yields the following universal relation for $S_{\uparrow\downarrow}(k)$,

$$S_{\uparrow\downarrow}(k \gg k_{\mathrm{F}}) = \left(\frac{\mathcal{I}}{Nk_{\mathrm{F}}} \right) \frac{k_{\mathrm{F}}}{4k} \left[1 - \frac{4}{\pi k_{\mathrm{F}}a} \left(\frac{k_{\mathrm{F}}}{k} \right) \right], \tag{3}$$

which is written in this way to show the explicit dependence on the dimensionless contact $\mathcal{I}/(Nk_{\mathrm{F}})$, where N is the total number of particles, k/k_{F} is the relative probe momentum and $1/(k_{\mathrm{F}}a)$ is the interaction strength. At unitarity, $a \to \infty$, the second term in the square brackets vanishes and $S(k)$ varies linearly with k_{F}/k. Rewriting Tan's relation in this way points to a pathway for experimental validation through Bragg spectroscopy [22].

Inelastic scattering experiments are well established as a means to probe both the dynamic and the static structure factors of many-body quantum systems [23]. The dynamic structure factor $S(k, \omega)$ characterizes the excitation spectrum of a many-body system and depends upon the particle–particle correlations in the system. Ultracold atoms are highly amenable to inelastic scattering through Bragg spectroscopy, which has previously been used to measure both the dynamic and the static structure factors [24–27] of atomic BECs. In ultracold Fermi gases, Bragg spectroscopy was used to measure both the dynamic and the static structure factors over the BEC–BCS crossover, albeit at a single momentum [9]. Bragg spectroscopy differs from rf spectroscopy in that it probes density–density correlations, whereas rf probes the single-particle spectral function $A(k, \omega)$ [28]. Additionally, Bragg spectroscopy avoids complications arising from final state interaction effects as no third atomic state is involved [29].

The resonant recoil frequency ω_{r} for Bragg scattering is the frequency at which both energy and momentum are simultaneously conserved in a two-photon scattering event. In the single-particle regime, this means that the energy difference between the two lasers used in Bragg scattering must be equal to the kinetic energy of the particle after gaining $\hbar k$ of momentum, where $k = |\mathbf{k}_1 - \mathbf{k}_2|$ is the difference in wave vectors of the the two Bragg laser beams. This leads to the Bragg condition $\omega_{\mathrm{r}} = \hbar k^2/(2m)$, where m is the mass of the scattered atoms. Since the mass of the particle comes into the recoil frequency, Bragg spectroscopy provides a means of distinguishing molecular dimers (or pairs) from free atoms, leading to a physically intuitive picture of how Bragg scattering can be used to extract the contact. As $\mathcal{I}$ physically represents the

IOP Institute of Physics Φ DEUTSCHE PHYSIKALISCHE GESELLSCHAFT

number of closely spaced pairs, these pairs may scatter from the Bragg lattice as single particles with mass $2m$ (twice the atomic mass). Hence they should show up as a peak in the excitation spectrum at half of the atomic recoil frequency and the size of this peak should be proportional to the contact. In real trapped systems, these peaks are broadened by a number of mechanisms and the contact can be obtained by the integrated response through $S(k)$ and equation (3).

The Bragg experiments we consider here are performed in the linear response regime, where the fraction of particles scattered is small compared with N and the duration of the Bragg pulse τ is short compared to the two-photon Rabi cycling period. In this limit, the momentum transferred to the cloud via the Bragg pulse is given by the convolution of the spectral components of the Bragg pulse with the difference between the positive and negative frequency dynamic structure factors [9, 30]

$$\Delta P(k, \omega) = \hbar k \frac{\Omega_{Br}^2}{2} \int [S(k, \omega') - S(-k, -\omega')] . \frac{\sin^2 [(\omega - \omega') \frac{\tau}{2}]}{(\omega - \omega')^2} d\omega', \qquad (4)$$

where Ω_{Br} is the two-photon Rabi frequency. Similarly, the energy transferred to the cloud via a Bragg pulse is given by

$$\Delta E(k, \omega) = \frac{\hbar \Omega_{Br}^2}{2} \int \omega' [S(k, \omega') - S(-k, -\omega')] . \frac{\sin^2 [(\omega - \omega') \frac{\tau}{2}]}{(\omega - \omega')^2} d\omega'. \qquad (5)$$

When the Bragg pulse is long, the sine-squared term in the integral becomes narrow compared with the features in the dynamic structure factor and contributes little to the shape of the measured spectra. Furthermore, as generally we will be concerned only with the integrals of Bragg spectra over the frequency ω, and the Bragg pulse duration is the same for all experiments, this convolution scales all of the measured quantities by the same amount. As this scaling cancels in our normalization procedure, we can ignore the convolution without affecting our analysis. Under this assumption, the momentum and energy transferred simplify to

$$\Delta P(k, \omega) = \hbar k \frac{\Omega_{Br}^2}{2} [S(k, \omega) - S(-k, -\omega)] \qquad (6)$$

and

$$\Delta E(k, \omega) = \hbar \omega \frac{\Omega_{Br}^2}{2} [S(k, \omega) - S(-k, -\omega)] , \qquad (7)$$

respectively, i.e. they differ by a factor of ω/k. Both the positive and the negative frequency structure factors are included here because, particularly at higher temperatures and lower momenta, atoms may absorb light from either of the Bragg lasers. We can easily account for this in a way that leaves only the positive component of the dynamic structure factor using the principle of detailed balancing, which states that in thermal equilibrium,

$$S(k, \omega) - S(-k, -\omega) = \left[1 - \exp\left(-\frac{\hbar \omega}{k_B T} \right) \right] S(k, \omega), \qquad (8)$$

where k_B is Boltzmann's constant. With this relation, we can extract the dynamic structure factor from either the measured momentum or energy transferred to the cloud by the sequence of Bragg pulses as k, ω and T are all known. Additionally, we can use the f-sum rule to link the area under the measured spectra to the true dynamic structure factor (section 4) [22]. Once the true dynamic structure factor is known, we can determine the static structure factor by integration

over ω,

$$S(k) = \frac{\hbar}{N} \int S(k, \omega) \mathrm{d}\omega. \tag{9}$$

This then allows us to obtain the contact directly through equation (3).

Traditionally, Bragg spectroscopy has been achieved by measuring $\Delta P(k, \omega)$ through measurements of cloud displacement after a short time of flight. A number of recent studies on Bose gases in lattices, however, have also made use of energy transfer Bragg spectroscopy through measurements of the cloud width [31–33]. Recently, we showed that both the first and the second moments of absorption images of clouds released immediately after the Bragg pulse can be used to obtain a measure of the dynamic structure factor [34]. In section 4, we compare these measurements to new determinations of $\Delta E(k, \omega)$ measured from increases in the size of trapped clouds, after allowing a sufficiently long time for re-equilibration. This method can offer improved signal-to-noise ratios under certain conditions, particularly at low momentum transfer [33].

3. Interaction dependence of the contact

The starting point of all of our Bragg experiments is an evaporatively cooled cloud containing $N \approx 3 \times 10^5$ ^{6}Li atoms in an equal mixture of the two lowest-lying ground states $|F = 1/2, m_F = \pm 1/2\rangle$ loaded into a far detuned optical dipole trap [35]. The cloud is prepared at a magnetic field of $834\,\mathrm{G}$, where elastic collisions are unitarity limited by the broad s-wave Feshbach resonance. Depending on the power and beam waists of the trapping laser, we can tune the mean harmonic confinement frequency over a large range and we have previously used this flexibility to study the dependence of $S(k)$ on the ratios k/k_F and $1/(k_F a)$ in order to experimentally verify the universal relation in equation (3) [22]. In that work, we also presented the static structure factor at $k = 4.8k_F$ as a function of $1/(k_F a)$ [9, 22], where we showed that normalizing the Bragg spectra using the f-sum rule greatly improves the accuracy of the measured structure factors. Combining these results with equation (3), we obtain the interaction dependence of the contact, which we present for the first time in figure 1 below, along with a zero-temperature calculation using a Gaussian pair fluctuation theory based on the many-body t-matrix approximation [36]. These Bragg spectroscopic measurements were taken using clouds prepared at a temperature of $T \lesssim 0.1T_F$ at unitarity, before being adiabatically swept to the different magnetic fields. The data are in good agreement with previous results [8, 20, 28] and show a strong increase in the contact on the BEC side of the Feshbach resonance.

The agreement between experiment and theory also suggests that our universal relation for the structure factor, equation (3), is reliable away from unitarity, up to $|1/(k_F a)| \sim 1$ at the momentum considered here ($4.8k_F$). For the largest value of $1/(k_F a) = +1.4$, the second term in square brackets of equation (3), which provides the first-order correction to $S(k)$ away from unitarity, is only 0.37, which is still significantly less than one and higher-order terms will be smaller again, so equation (3) is still quite reliable in this region. We note that the second term in brackets in equation (3) does not depend on k_F, so its applicability requires that $a \gg k^{-1}$.

4. Temperature dependence of the contact

To investigate the temperature dependence of the contact, we load the atoms at unitarity ($834\,\mathrm{G}$) into a deep single beam optical dipole trap so that even the higher temperature clouds will be
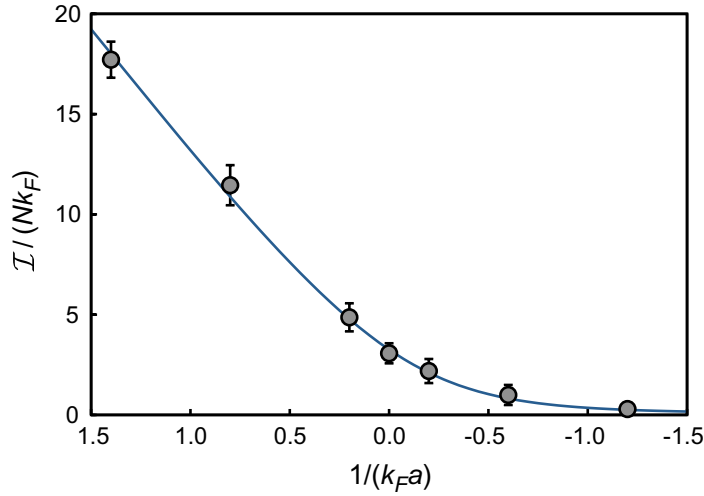
Figure 1. Contact, $\mathcal{I}/(Nk_{\mathrm{F}})$, as a function of the dimensionless interaction parameter, $1/(k_{\mathrm{F}}a)$. Data points are obtained from static structure factor measurements at $k = 4.8k_{\mathrm{F}}$ [22] and equation (3). The solid line is a zero-temperature calculation based on a Gaussian pair fluctuation theory [36].

confined in the harmonic region of the trapping potential. This deep trap also allows us to keep atoms trapped after the Bragg pulse has been applied as the trap depth $U \approx 90\,\mathrm{kHz}$ is much larger than the recoil energy $\hbar\omega_{\mathrm{r}}$ and the Fermi energy ($U \approx 12E_{\mathrm{F}}$). This allows us to measure the energy imparted by the Bragg pulse after a long hold time for re-equilibration, as discussed in section 4.2. We vary the cloud temperature by suddenly switching off the dipole trap for a variable time before quickly ramping it on and holding the cloud for $400\,\mathrm{ms} \gg 1/\bar{\omega}$, where $\bar{\omega} = 2\pi \times 71.5\,\mathrm{s}^{-1}$, to re-thermalize [7]. During the release, a magnetic field gradient is applied that levitates the atoms against gravity and minimizes the centre-of-mass sloshing that would otherwise occur upon recapture. In this way, we can repeatably heat the cloud to temperatures of up to $T = 1.1\,T_{\mathrm{F}}$ without losing atoms.

4.1. Temperature measurement at unitarity

The measurement of temperature in strongly interacting Fermi gases poses significant challenges to experiments due to the lack of a finite-temperature analytic model for the density profile [37]. A number of techniques have been developed to obtain temperatures of spin-balanced Fermi gases, each with its advantages and disadvantages. These include the determination of an empirical temperature $\tilde{T}$ from fits of an ideal gas Thomas–Fermi profile to clouds imaged at unitarity [7]; adiabatic magnetic field sweeps to the weakly interacting regimes where perturbative models are accurate [38, 39]; measurements of the entropy and energy and the fundamental thermodynamic identity $1/T = \partial S/\partial E$ [40]; and the use of a small admixture of another weakly interacting species that can act as a thermometer [11, 41]. The latter method is perhaps most elegant and reliable but requires the simultaneous cooling of a second species in the apparatus, which can pose difficulties.

We determine the temperature of clouds at unitarity following the techniques developed in the Duke group [7, 37] by fitting finite-temperature Thomas–Fermi profiles to images of
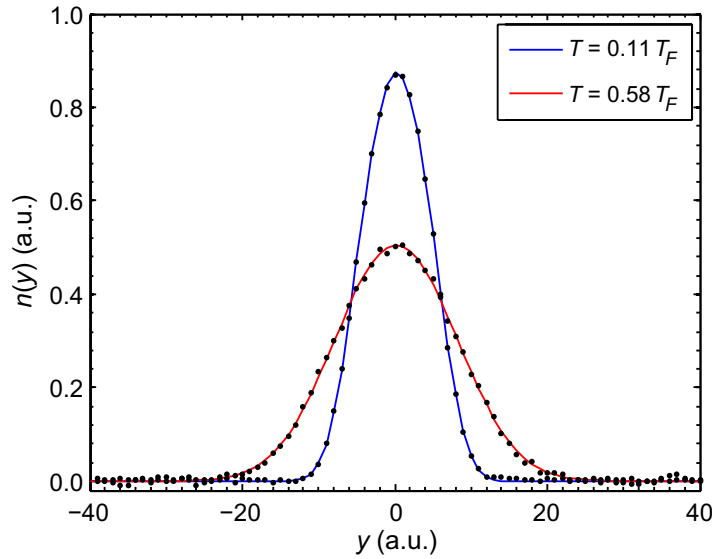
Figure 2. 1D line profiles $n(y)$ of clouds prepared at two different temperatures at unitarity along with finite-temperature Thomas–Fermi fits. The fitted function is used to extract empirical temperature $\tilde{T}$, which gives an estimate of the true temperature shown in the inset in units of the Fermi temperature T_{F}.

clouds after 2 ms expansion to obtain $\tilde{T}$. The empirical temperature provides a robust, but model-dependent, estimate of the true temperature $T/T_{\mathrm{F}} = \sqrt{1+\beta}\,\tilde{T}$, where $\beta = -0.617$ is a universal parameter [42]. Because of the model dependence, we also calibrate our temperatures with independent measurements of the mean energy per particle at unitarity. These are compared to theoretical calculations using a below threshold version of the Nozières–Schmitt–Rink (NSR) scheme [43], based on a many-body t-matrix approximation, for the equation of state of harmonically trapped Fermi gases [44]. While this does imply a model dependence, this NSR theory has been shown to provide excellent agreement with the experimentally measured equation of state over nearly the full range of temperatures that we study [11, 45] and thus provides a reliable benchmark for the $\tilde{T}$ measurements.

Figure 2 shows examples of fits of a Thomas–Fermi profile to one-dimensional (1D) density profiles $n(y)$ of two clouds that yield temperatures of $0.11\,T_{\mathrm{F}}$ and $0.58\,T_{\mathrm{F}}$, respectively. Each profile is obtained from the average of five absorption images taken under identical conditions. The quality of the fits is very good and the uncertainties in fitted empirical temperatures are generally at the level of a few per cent. The conversion from the empirical temperature to the true temperature, however, is subject to systematics (e.g. the density profile below the critical temperature for superfluidity is not simply a scaled Thomas–Fermi profile [46]) and as such needs to be calibrated in an independent way. In figure 3, we plot the measured mean energy per particle as a function of the temperature obtained from the fitted $\tilde{T}$ and compare these to the calculated mean energy per particle. In a unitary cloud, the mean energy per particle is directly proportional to the mean square cloud width and the total energy is shared equally between kinetic and potential energies, independent of temperature. The solid line is a calculation based on the NSR theory [3] and the dash-dotted line is taken from a power-law fit to model-independent temperature measurements obtained from
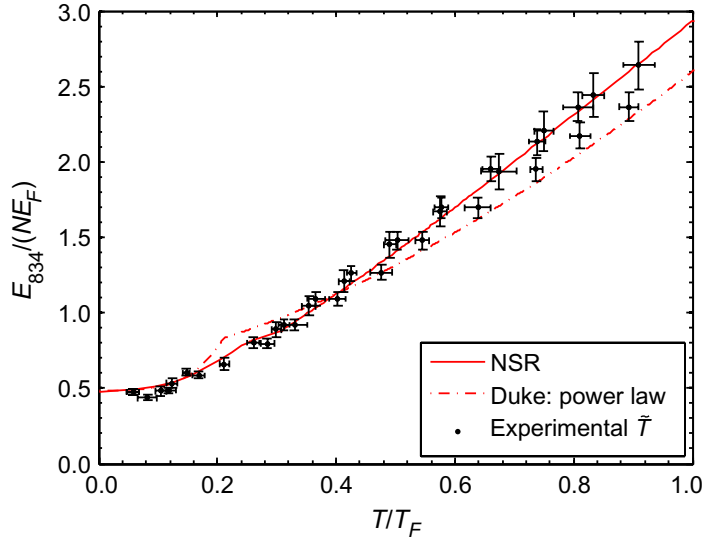
Figure 3. Comparison of the measured mean energy per particle at unitarity with the energy calculated using a NSR theory [3] and the power-law fit to the Duke results [37]. The position along the horizontal axis of the experimental data is determined from fits of the empirical temperature $\tilde{T}$ and the energy is obtained through measurements of the mean-square width of trapped clouds.

the fundamental thermodynamic identity $1/T = \partial S/\partial E$, where S is the entropy, performed by the Duke group [37, 40]. Our results lie close to the NSR theory and slightly above the power-law calibration curve obtained from the Duke experiments. We obtain an estimate of the uncertainty in our temperature measurement from the mean difference between the temperatures obtained from the fitted $\tilde{T}$ and the temperature corresponding to a cloud with the same mean energy per particle.

Temperature measurement away from unitarity is even more difficult in spin balanced systems, particularly on the BEC side of the Feshbach resonance where models, such as the NSR, become less reliable. For this reason, we instead use the entropy to parametrize the data. We obtain the entropy by isentropically sweeping the magnetic field either to the far BCS side, where $1/(k_F a) = -1.5$, or to unitarity, where we measure the mean square cloud width, which we relate to the entropy via the NSR model. At $1/(k_F a) = -1.5$, the NSR entropy is almost identical to the entropy of an ideal gas, differing by a maximum of $\approx 4\%$ for temperatures below $0.2\,T_F$.

4.2. Bragg spectroscopy: the energy transfer method

Here, we describe the procedure we used for energy transfer Bragg spectroscopy. Bragg scattering is achieved by illuminating ^{6}Li clouds with two laser beams that have a small tunable frequency difference ω that intersect at an angle of $\theta = 49°$. This creates a standing wave that moves with velocity ω/k, where $k = 4\pi \sin(\theta/2)/\lambda$ and $\lambda = 671$ nm is the wavelength of the light used for Bragg scattering. In combination with the trap parameters and atom numbers we use, this gives a relative probe momentum of $k = 2.7k_F$, which enhances the contribution of $S_{\uparrow\downarrow}(k)$ to $S(k)$ according to equation (3). This leads to an atomic recoil frequency of 51.6 kHz.

Bragg spectroscopic studies typically measure the momentum transferred to a cloud as the observable through the number of scattered atoms or the centre of mass displacement [9, 24]. We recently carried out a measurement of the temperature dependence of the contact [34] using Bragg spectroscopy. In that work, we showed that measuring both the first $\langle x \rangle$ and the second moments $\langle x^2 \rangle$ of atom clouds after immediate release from the confining potential can provide quantitative information about the dynamic structure factor. Here, we take this idea further and determine the energy transferred to the cloud from measurements of the increase in the mean square cloud width, $\Delta \sigma^2$, once the atoms have re-equilibrated in the trap, following a long hold time after the Bragg pulse. Due to the high elastic collision rates in trapped clouds, the energy imparted by the Bragg pulse is rapidly distributed among all of the atoms through collisions. The Bragg pulse may also induce centre of mass oscillations; however, after a long hold time in the trap, these oscillations damp out to below our detection limit due to the slight anharmonicity of our trapping potential. After the oscillations have damped, the width of the cloud alone provides a measure of the energy imparted. The advantage of this method over our earlier method is that it does not require *a priori* knowledge of a reference centre of mass position. As such, this method is insensitive to small (micron) scale drifts in the trap position over the time it takes to obtain a Bragg spectrum, which can be a limitation when measuring cloud displacement. The main weakness of this method is that the cloud width (at zero temperature) varies as $N^{1/6}$. As this is a very weak dependence and typical shot-to-shot atom number fluctuations can be made relatively small, this does not pose a serious constraint. At higher temperatures, the N dependence eventually disappears in the classical gas limit.

This technique relies on having a trap deep enough such that no atoms will be lost following the Bragg pulse. We achieve this using a 1064 nm optical dipole trap operated at 8 W, with beam waists of 600 μm by 170 μm. The resulting trap has harmonic confinement frequencies of $(\omega_x, \omega_y, \omega_z)/2\pi = (24.5, 65, 230)$ Hz ($\bar{\omega} = 71.5$ Hz) and a depth of almost twice the atomic recoil energy. In all of our Bragg spectra, at temperatures of up to 1.1 T_F, we can detect no loss of atoms from the trap after the Bragg pulse.

We obtain spectra by applying a 200 μs Bragg pulse and measuring the cloud width after 400 ms hold time in the trap. As this hold time is very long compared to $1/\bar{\omega}$ and the elastic collision rate is unitarity limited and hence very large [47], this is ample time for the energy to distribute itself equally among all available degrees of freedom. This allows us to measure the increase in cloud width in both the x- and y-directions from a single shot, whereas our previous Bragg studies, based on momentum transfer, only measured a signal in one dimension. This hold time is also long enough that we observe no residual centre of mass motion. Additionally, the measured width increase after a long hold time is independent of the direction of the Bragg scattering wave vector ($\mathbf{k} = \mathbf{k}_1 - \mathbf{k}_2$), removing the constraint of imaging perpendicular to $\mathbf{k}$.

Absorption images of clouds after the long hold time yield symmetric 2D density profiles $n(x, y)$. From these we can integrate over either direction to obtain 1D line profiles $n(x)$ and $n(y)$. To determine the second moments of these, we fit Gaussian profiles to the cloud and take the second moment of the fitted functions. Analysing the data in this way is much less sensitive to shot noise in the individual pixels, which was present in our previous work [34]. At low temperatures, however, Gaussian profiles do not provide a particularly good fit to the cloud shape and, in the worst case, the second moment of the fitted Gaussians can be up to 15% higher than the true moment extracted from the data points. However, as we are only concerned with relative increases in the cloud energy rather than the absolute energy, this systematic error
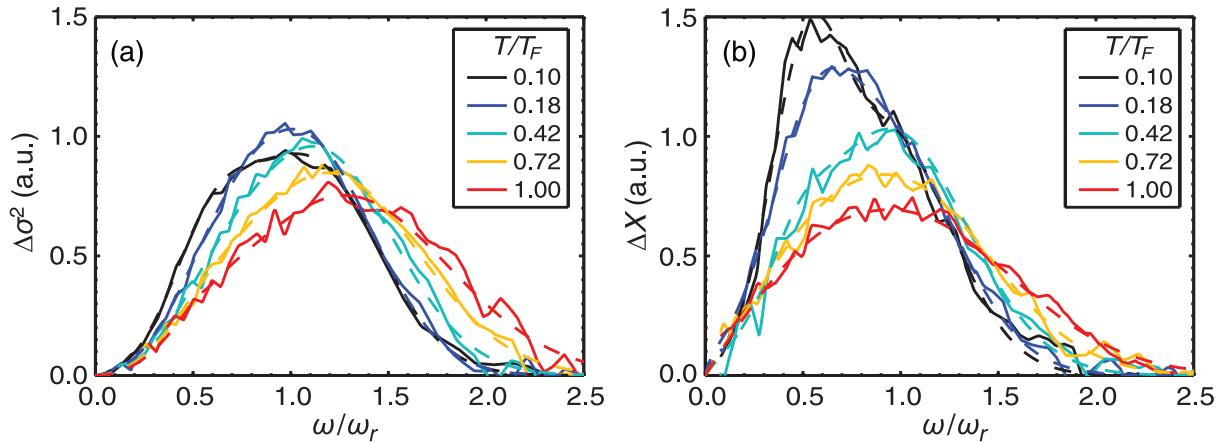
Figure 4. Bragg spectra for a unitary Fermi gas showing (a) the increase in mean square cloud size (energy transferred) after $400\,\text{ms}$ hold time in the trap and (b) the centre of mass displacement (momentum transferred) following immediate release from the trap [34] as a function of the Bragg frequency ω.

provides essentially no contribution to the static structure factors we determine, as discussed below.

The key to this insensitivity to the shape of the fitted function lies in the fact that we independently normalize all our measured spectra via the f-sum rule. Thus it is only the relative nonlinearity, in the second moment of the Gaussian fit as a function of T, compared to the second moment of the true distribution, that contributes to an error in the measured structure factors. We estimate this nonlinearity by comparing the temperature derivative of the second moment of a Gaussian fitted to a finite temperature Thomas–Fermi profile with the temperature derivative of the second moment of the Thomas–Fermi distribution itself. For the coldest clouds and the largest energy increases we observe, the nonlinearity leads to an error in the relative energy increase of $\approx 3\%$. This is already smaller than the uncertainty in our measurement of the relative energy increase and, when propagated through our analysis procedure to determine the static structure factor and contact, the resulting error is less than 1%, well below other uncertainties arising from atom number fluctuations and imperfect imaging. The Gaussian fit therefore provides a simple and robust way to determine the relative increase in cloud energy and introduces effectively no additional contributions to our overall measurement uncertainty.

Figure 4(a) (solid lines) shows Bragg spectra of unitary clouds obtained from measurements of the energy transferred at the five temperatures listed in the legend. These spectra are the average of the relative increase in width in both the x- and y-directions, averaged for four spectra. These spectra appear quite different in shape to traditional spectra based on measurements of the momentum transferred (also the average of four spectra) shown in figure 4(b) [9, 34], as the energy spectra represent the dynamic structure factor multiplied by the energy $\hbar\omega$. The raw data in figure 4(b) display considerably less scatter than the second moment data of our previous measurements [34].

As discussed in section 2, both types of Bragg spectra can provide quantitative information about the dynamic and static structure factors and hence the contact. Figures 4(a) and (b) also show fits to the measured spectra (dashed lines) that we use for further evaluation. For the

energy spectra in figure 4(a), the fitted function is of the form

$$F_E(\omega) = \omega \cdot (1 - e^{-\hbar\omega/k_B T}) \cdot [c_a e^{-[(\omega-\omega_a)^2]/2\sigma_a^2} + c_b e^{-[(\omega-\omega_b)^2]/2\sigma_b^2}]. \tag{10}$$

The first term in brackets accounts for detailed balancing, and the two Gaussian functions in square brackets represent the dynamic structure factor $S(k, \omega)$. The first Gaussian is centred on $\omega_a \approx \omega_r/2$ to account for pair excitations and the second is centred on $\omega_b \approx \omega_r$ for atomic excitations. The amplitudes $c_{a,b}$, widths $\sigma_{a,b}$ and centre positions $\omega_{a,b}$ of the two Gaussians are used as fit parameters. For the momentum spectra shown in figure 4(b), we fit an almost identical function $F_P(\omega)$, which does not have the pre-factor of ω, i.e. $F_P(\omega) \equiv F_E(\omega)/\omega$.

These fitted functions provide information about the relative response at both pair and atomic excitation frequencies. To establish the absolute amplitudes, we require that the fitted Gaussians satisfy the f-sum rule [23] such that

$$\hbar \int \omega \cdot [c_a' e^{-(\omega-\omega_a)^2/2\sigma_a^2} + c_b' e^{-(\omega-\omega_b)^2/2\sigma_b^2}] d\omega = N\omega_r. \tag{11}$$

The new coefficients c_a' and c_b' are just the original coefficients scaled by the same factor to satisfy equation (11). With these new coefficients, the two Gaussians provide a good representation of the dynamic structure factor [34, 48] that can be integrated to obtain $S(k)$ and hence the contact.

We have also obtained Bragg spectra using energy transfer measurements at magnetic fields of 780 G, $1/(k_F a) = 1.1$ and 860 G, $1/(k_F a) = -0.4$ on the BEC and BCS sides of the Feshbach resonance, respectively. The same fitting procedure described above gives the dynamic structure factors, which are plotted for all three cases in figures 5(a)–(c) for the unitary, BCS and BEC cases, respectively. These spectra were obtained at a range of different cloud temperatures; however, due to the difficulty in quantifying temperatures on the BEC side of the resonance, we instead distinguish the spectra by the cloud entropy S. For spectra on the BCS side, this was determined by isentropically sweeping the magnetic field to $1/(k_F a) = -1.5$ and measuring the cloud (mean square) size relative to the Fermi radius. We convert the size to entropy using an NSR calibration curve for $1/(k_F a) = -1.5$. At unitarity, we apply the same procedure with an NSR calibration curve at $1/(k_F a) = 0$ to obtain the entropy. The entropy for clouds on the BEC side is obtained after isentropically sweeping the magnetic field to unitarity and using the unitarity calibration. The uncertainties in our temperature measurement and entropy calibration procedure lead to uncertainties in the quoted entropies of approximately 7%.

The dashed lines in figure 5 are the Gaussian fits for $S(k, \omega)$ and the solid lines are calculations based on the QVE to second order [49]. The virial expansion is only strictly reliable when the fugacity is a small parameter that corresponds to temperatures $T \gtrsim T_F$; however, it qualitatively captures the main features of $S(k, \omega)$ down to $T \sim 0.5\,T_F$, or $S \sim 3.6(Nk_B)$ at unitarity. In figure 5(a), we plot the unitary dynamic structure factors obtained from averaging the data of figure 4. The inset shows a comparison of the three highest temperature spectra with the QVE calculations, which display very good agreement. On the BEC side of the Feshbach resonance, figure 5(b), we show four dynamic structure factors measured at relatively low entropy. Only the Gaussian fits for the structure factors are plotted as the cloud temperatures were too low for quantitative comparisons with the QVE. Also, for the lowest temperatures, the Gaussian fit for the molecular peak at $\omega_r/2$ becomes a poor approximation. On the BCS side, figure 5(c), the Gaussian fits are plotted with the two coldest (lowest entropies) spectra and the QVE is plotted for the two hottest (highest entropies) spectra. The QVE shows very good quantitative agreement with the data.
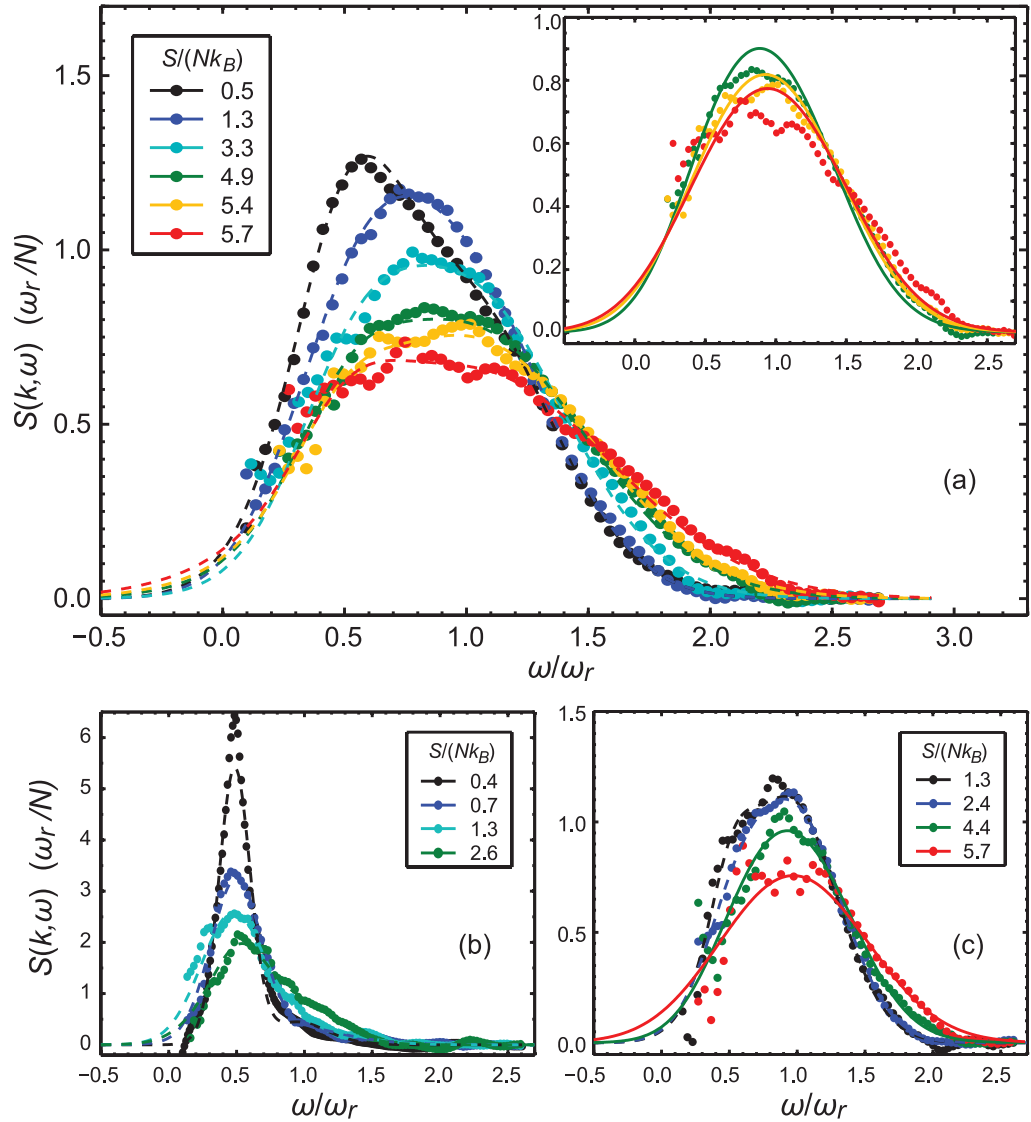
Figure 5. $S(k, \omega)$ from selected Bragg spectra at different interaction strengths and entropies. Data points are the filled circles and the solid (dashed) lines are the results of QVE calculations (Gaussian fits) for the dynamic structure factor. (a) $S(k, \omega)$ at unitarity for a range of entropies with the Gaussian fits to the data. Inset: $S(k, \omega)$ for the three highest entropies along with QVE calculations. (b) Data and Gaussian fits to $S(k, \omega)$ at $1/(k_F a) = +1.1$. (c) Data, Gaussian fits and QVE results for $S(k, \omega)$ at $1/(k_F a) = -0.4$.

With these dynamic structure factors, we can determine the static structure factors and contact according to equation (3), which are plotted in figure 6. The static structure factors shown in figure 6(a) decay as the entropy (temperature) increases, in reasonable agreement with the QVE theory. The BEC data appear to lie consistently above the theoretical predictions, most likely due to the inaccuracy in approximating the molecular peak of the dynamic structure factor by a Gaussian [48]. Equation (3) also provides the contact shown versus the entropy
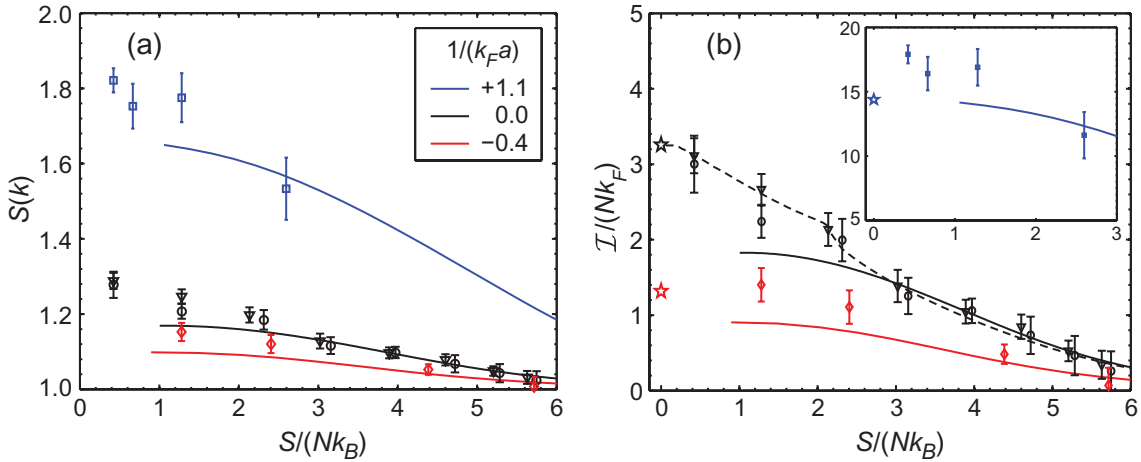
Figure 6. Measured and calculated static structure factor (a) and contact (b) versus entropy at $1/(k_Fa) = +1.1$ (blue squares), 0 (black circles and triangles) and -0.4 (red diamonds). The points are the experimental data and the solid lines are calculations based on the QVE. At unitarity, the circles are data obtained from energy transfer measurements only and the triangles are from our earlier work [34]. The dashed black line and zero-temperature contacts (stars) shown in (b) are obtained from a NSR calculation [36].

in figure 4(b) along with the virial calculations and the NSR theory (green) at unitarity. The main plot shows the contact obtained from the unitarity and BCS spectra, both of which agree well with the QVE calculations (black and red) at higher entropies above $3.6\ S/(Nk_B)$. At unitarity, the NSR calculation provides the contact at low entropies and we find good agreement between the data and predicted values. Also shown in figure 6(b) are our earlier contact data, obtained from the first and second moments after immediate release (triangles) [34], where the temperature has been converted into entropy using the NSR calibration. The inset depicts just the contact on the BEC side and the stars indicate the calculated zero-temperature values of the contact.

It is interesting to compare the two Bragg spectroscopic methods for measuring the contact at unitarity. The circles in Figure 6 are data obtained from measurements of the energy transfer alone and the triangles are our earlier data of the first and second moments a short time after the Bragg pulse [34]. Both methods provide very similar results with comparable error bars and show the monotonic decay of $\mathcal{I}/(Nk_F)$ with increasing temperature, in good agreement with theory. Despite the less noisy appearance of the spectra obtained through energy transfer Bragg spectra in figure 4(a), the resulting error bars for the measured contact are similar to those of our earlier data. The error bars for both sets of data are the standard deviations of the static structure factor and contact from the individual spectra. The reason for the comparable uncertainties in the energy-transfer-based contact measurements is still under investigation, but is most likely due to excessive atom number fluctuations in some of the individual spectra, combined with the fact that these spectra are divided by ω, which increases the noise at low frequencies relative to momentum transfer spectra.

The measured contact on the BCS side is in reasonable agreement with the theoretical predictions, as expected from the agreement seen in the dynamic structure factors, figure 5(c). On the BEC side, the measurements are above the theoretical predictions; however, uncertainties in the data are large as the spectra are dominated by the pairing peak, which we approximate with a Gaussian. It is also possible that the universal relation equation (3) at this relatively low momentum of $2.7 k_F$ is beginning to break down at $1/(k_F a) = +1.1$. The second term in brackets in equation (3) here approaches 0.5, which indicates that higher-order terms may start to become significant.

As discussed in our earlier work, theoretical calculations of the contact at unitarity have each predicted different behaviours near the critical temperature for superfluidity $T_c \approx 0.2 T_F$ ($S/N k_B \approx 2$) [36, 50, 51]. Unfortunately, with the uncertainties in our measurements, we cannot identify one theory as being more accurate than another. However, it appears that the energy-based contact measurements are slightly lower near T_c. With improvements to the atom number reproducibility, and a closer study of the critical region near T_c, we are optimistic that the energy transfer method of Bragg spectroscopy will provide the improved accuracy required to resolve the discrepancies between different theories.

It is interesting to note that $\mathcal{I}$ is significant for temperatures well above T_c on both sides of the Feshbach resonance and that pair correlations build up steadily below T_F. At the momentum we have studied ($2.7 \hbar k_F$), the $1/k^4$ momentum tail, at the heart of the contact, dominates the pair-correlation function. The relationship between these short-range correlations and medium-range correlations on the many-body length scale ($\sim k_F^{-1}$) is still unclear but is the subject of ongoing research [50]. Measurements of the pair size in a unitary Fermi gas [29] suggest that this is the important scale to probe for the existence of a pseudogap phase and preformed pairs that form above T_c [53]. Bragg spectroscopy with lower momentum transfer will be able to probe pairing in this region, but becomes more complicated as the assumption of scattering into unoccupied states, which allowed us to approximate the spin-parallel component of the static structure factor as 1, is no longer valid and $S_{\uparrow\uparrow}(k) < 1$. However, additional Bragg measurements that probe the magnetic structure factor $S_M(k) = S_{\uparrow\uparrow}(k) - S_{\uparrow\downarrow}(k)$, in combination with measurements of $S(k) = S_{\uparrow\uparrow}(k) + S_{\uparrow\downarrow}(k)$, could provide a means of unambiguously determining both the spin-parallel and spin-antiparallel components [19, 52]. This would allow us to measure spin anti-parallel correlations and probe pairing in the pseudogap region [53]. Energy transfer Bragg spectroscopy may prove to be valuable at these lower momenta [33].

5. Conclusions

We have presented a study of the interaction and temperature dependence of Tan's universal contact in strongly interacting Fermi gases using Bragg spectroscopy. We have described our procedures for preparing ultracold ^{6}Li gases at a range of temperatures and for obtaining quantitative measures of the contact from Bragg spectra. Our results indicate that the high momentum tail of the pair-correlation function is significant at temperatures well above T_c, in good agreement with theoretical predictions. The QVE was seen to provide an accurate determination of the dynamic structure factor and contact at temperatures $T \gtrsim 0.5 T_F$. More extensive studies of the region near T_c are needed in order to resolve the discrepancies between different theoretical approaches, and the methods we have shown here may have the capability of achieving that in the near future. Bragg experiments at lower momentum ($k \sim k_F$) represent

IOP Institute of Physics ⓘ DEUTSCHE PHYSIKALISCHE GESELLSCHAFT

an emerging direction that will enable us to probe the regime where pseudogap behaviour has been observed but is still the subject of active research [11, 50, 53].

Acknowledgment

References

[1] Heiselberg H 2001 *Phys. Rev.* A **63** 043606
[2] Ho T-L 2004 *Phys. Rev. Lett.* **92** 090402
[3] Hu H, Drummond P D and Liu X-J 2007 *Nat. Phys.* **3** 469
[4] Jochim S, Bartenstein M, Altmeyer A, Hendl G, Riedl S, Chin C, Hecker-Denschlag J and Grimm R 2003 *Science* **302** 2101
[5] Greiner M, Regal C A and Jin D S 2003 *Nature* **426** 537
[6] Zwierlein M W, Abo-Shaeer J R, Schirotzek A, Schunck C H and Ketterle W 2005 *Nature* **435** 1047
[7] Kinast J, Turlapov A, Thomas J E, Chen Q, Stajic J and Levin K 2005 *Science* **307** 1296
[8] Partridge G B, Strecker K E, Kamar R I, Jack M W and Hulet R G 2005 *Phys. Rev. Lett.* **95** 020404
[9] Veeravalli G, Kuhnle E D, Dyke P and Vale C J 2008 *Phys. Rev. Lett.* **101** 250403
[10] Horikoshi M, Nakajima S, Ueda M and Mukaiyama T 2010 *Science* **327** 729
[11] Nascimbène S, Navon N, Jiang K J, Chevy F and Salomon C 2010 *Nature* **463** 1067
[12] Navon N, Nascimbène S, Chevy F and Salomon C 2010 *Science* **328** 729
[13] Giorgini S, Pitaevskii L P and Stringari S 2008 *Rev. Mod. Phys.* **80** 1215
[14] Tan S 2008 *Ann. Phys.* **323** 2952
[15] Tan S 2008 *Ann. Phys.* **323** 2971
[16] Tan S 2008 *Ann. Phys.* **323** 2987
[17] Braaten E and Platter L 2008 *Phys. Rev. Lett.* **100** 205301
[18] Zhang S and Leggett A J 2009 *Phys. Rev.* A **79** 023601
[19] Combescot R, Giorgini S and Stringari S 2006 *Europhys. Lett.* **75** 695
[20] Werner F, Tarruell L and Castin Y 2009 *Eur. J. Phys.* B **68** 401
[21] Stewart J T, Gaebler J P, Drake T E and Jin D S 2010 *Phys. Rev. Lett.* **104** 235301
[22] Kuhnle E D, Hu H, Liu X-J, Dyke P, Mark M, Drummond P D, Hannaford P and Vale C J 2010 *Phys. Rev. Lett.* **105** 070402
[23] Pines D and Nozières P 1966 *The Theory of Quantum Liquids* vol 1 (New York: Benjamin)
[24] Stenger J, Inouye S, Chikkatur A P, Stamper-Kurn D M, Pritchard D E and Ketterle W 1999 *Phys. Rev. Lett.* **82** 4569
[25] Stamper-Kurn D M, Chikkatur A P, Goerlitz A, Inouye S, Gupta S, Pritchard D E and Ketterle W 1999 *Phys. Rev. Lett.* **83** 2876
[26] Zambelli F, Pitaevskii L P, Stamper-Kurn D M and Stringari S 2000 *Phys. Rev.* A **61** 063608
[27] Steinhauer J, Ozeri R, Katz N and Davidson N 2002 *Phys. Rev. Lett.* **88** 120407
[28] Stewart J T, Gaebler J P and Jin D S 2008 *Nature* **454** 744
[29] Schunck C H, Shin Y, Schirotzek A and Ketterle W 2008 *Nature* **454** 739
[30] Brunello A, Dalfovo F, Pitaevskii L, Stringari S and Zambelli F 2001 *Phys. Rev.* A **64** 063614
[31] Clément D, Fabbri N, Fallini L, Fort C and Inguscio M 2009 *Phys. Rev. Lett.* **102** 155301
[32] Clément D, Fabbri N, Fallini L, Fort C and Inguscio M 2009 *New J. Phys.* **11** 103030
[33] Ernst P T, Götze A, Krauser J S, Pyka K, Lühmann D-S, Pfannkuche D and Sengstock K 2009 *Nat. Phys.* **6** 56

[34] Kuhnle E D, Hoinka S, Dyke P, Hu H, Hannaford P and Vale C J 2011 *Phys. Rev. Lett.* **106** 170402

[35] Fuchs J, Duffy G J, Veeravalli G, Dyke P, Bartenstein M, Vale C J, Hannaford P and Rowlands W J 2007 *J. Phys. B: At. Mol. Opt. Phys.* **40** 4109

[36] Hu H, Liu X-J and Drummond P D 2011 *New J. Phys.* **13** 0035007

[37] Luo L and Thomas J E 2009 *J. Low Temp. Phys.* **154** 1

[38] Carr L D, Shlyapnikov G V and Castin Y 2004 *Phys. Rev. Lett.* **92** 150404

[39] Hu H, Liu X-J and Drummond P D 2006 *Phys. Rev.* A **73** 023617

[40] Luo L, Clancy B, Joseph J, Kinast J and Thomas J E 2007 *Phys. Rev. Lett.* **98** 080402

[41] Spiegelhalder F M, Trenkwalder A, Naik D, Hendl G, Schreck F and Grimm R 2009 *Phys. Rev. Lett.* **103** 223203

[42] Gandolfi S, Schmidt K E and Carlson J 2011 *Phys. Rev.* A **83** 041601

[43] Nozières P and Schmitt-Rink S 1985 *J. Low Temp. Phys.* **59** 195

[44] Hu H, Liu X-J and Drummond P D 2006 *Europhys. Lett.* **74** 574

[45] Hu H, Liu X-J and Drummond P D 2010 *New J. Phys.* **12** 063038

[46] Ketterle W and Zwierlein M W 2008 *Ultracold Fermi Gases, Proc. Int. School Phys. 'Enrico Fermi', Course CLXIV, Varenna* ed M Inguscio, W Ketterle and C Salomon (Amsterdam: IOS Press) p 95

[47] Gehm M E, Hemmer S L, O'Hara K M and Thomas J E 2003 *Phys. Rev.* A **68** 011603

[48] Zou P, Kuhnle E D, Vale C J and Hu H 2010 *Phys. Rev.* A **82** 061605

[49] Hu H, Liu X-J and Drummond P D 2010 *Phys. Rev.* A **81** 033630

[50] Palestini F, Perali A, Pieri P and Strinati G C 2010 *Phys. Rev.* A **82** 021605

[51] Enss T, Haussmann R and Zwerger W 2011 *Ann. Phys.* **326** 770

[52] Guo H, Chien C-C and Levin K 2010 *Phys. Rev. Lett.* **105** 120401

[53] Gaebler J P, Stewart J T, Drake T E, Jin D S, Perali A, Pieri P and Strinati G C 2010 *Nat. Phys.* **6** 569